CrossMark

A new device for stress monitoring in continuously welded rails using bi-directional strain method

Ganzhong Liu[1] · Hao Liu[1] · Anqi Wei[1] · Jieling Xiao[1] · Ping Wang[1] ·
Shaozheng Li[1]

Abstract The technology of continuously welded rails (CWRs) is important in modern railway track structures. To measure rail stress, resistance strain gauges are preferred due to their good stability, sensitivity, and resistance to external interference. Based on the bi-directional strain method, we present a new method for measuring longitudinal rail stress using resistance strain gauges and develop a monitoring device for rail stress to realize long-term and multi-point measurement. Also relevant experimental verification and analysis are conducted. Results indicate that under various constraints the rail stress–strain values can be calculated just with the measured total longitudinal strain and total vertical strain. Considering the measurement error caused by sectional feature of sensors, we put forward a correction equation applicable to different stress conditions. Although the temperature values of the four full-bridge stress gauges can offset each other, the measurement error caused by rail flexural strain can also be eliminated to a certain extent at the same time, the non-uniform distribution of rail cross section temperature and unbalanced flexural strain still affect the measurement error. The experimental results also show that the developed rail-stress-monitoring sensor is suitable for measuring rail stress with reliable working performance.

1 Introduction

Continuously welded rails (CWRs) are an important technology in modern railway track structures. Nowadays, most new railways worldwide belong to super long continuously welded rail tracks. In addition, along with the rapid development of high-speed railways in recent years, new technologies in track structure have been widely used for ballastless tracks, large-sized welded turnouts, CWRs on long-span bridges, etc. As there is an additional longitudinal rail force caused by track-bridge interaction, it poses important challenges to preventing the expansion and breaking of CWRs, especially track buckling and breakage on long-span bridges which severely threat the track structures of high-speed railways based on ballastless tracks [1–3]. In high-temperature seasons, an excessively high longitudinal tension in rail bars may cause track buckling, lifting, rail-pad shifting, part damage and malfunction, etc. In low-temperature seasons, rail bars under an excessively high longitudinal tension are likely to cause track breakage. The accurate measurement of longitudinal rail stress and rail temperature is the key to scientific evaluation, management and maintenance of CWRs [4, 5].

On the basis of physical principles that rail materials have different mechanical, acoustical, electromagnetic, and material properties under different stresses, many researchers have tried to measure the longitudinal force in rail bars using the methods such as the strain method, flexural method, Barkhausen noise analysis (BNA) method, X-ray method, magnetic permeability method, and

✉ Jieling Xiao
xjling@swjtu.cn

1 MOE Key Laboratory of High-speed Railway Engineering, School of Civil Engineering, Southwest Jiaotong University, No. 111 of the North Second Ring Road, Chengdu 610031, China

ultrasonic method [6–11]. In 1992, Herzog developed a longitudinal stress measurement (LSM) process and put forward a patented method for measuring the fastening-down temperature of rails. In the field of rail thermal and residual stress measurements, there are a number of important techniques have been developed over the years, including rail uplifting or VERSE [12], neutron diffraction [13], magneto-elastic methods or MAPS [14], Rayleigh wave polarization measurements [15], nonlinear ultrasonic measurements [16], and the hole drilling method [17]. However, subject to limitations such as diversified rail-section sizes, weather, temperature, load complexity, measurement continuity, and in situ nondestructive tests, the above-mentioned methods still remain impractical for monitoring rail stress of CWRs.

Since the equipment used to measure longitudinal force in rails according to the strain method is simple and suitable for long-term monitoring, many researchers have adopted this method to detect and study the longitudinal force in CWRs on bridges [18, 19]. There are mainly two kinds of sensors for detecting longitudinal force in CWRs, resistance strain gauges and fiber Bragg grating sensors. The resistance strain gauges are widely used as traditional testing devices. For instance, Feng et al. [20, 21] used resistance strain gauges in a long-term monitoring of CWR sections from Beijing-Shanghai high-speed rail line on the bridges over Beijing-Hangzhou Grand Canal. LB Foster Salient Systems, a company in the U.S., applied the strain method to design a monitoring system [22, 23] for rail thermal expansion and longitudinal force. However, limited by CWRs' locking, crawling and temperature action mechanisms, and monitoring timeliness, unidirectional strain measurements cannot well monitor the rail temperature force in long-term operation conditions.

In this study, by analyzing the stress–strain relations of CWRs, we present a measuring method for longitudinal rail stress based on the bi-directional strain method, develop a rail-stress-monitoring device for long-term and multi-point measurements, and provide relevant indoor experimental verification.

2 Principles of bi-directional strain method in measuring rail stress

2.1 Analysis of the states of rail stress and strain

2.1.1 Rail stress–strain relation under the changes of rail temperature

As the deformation of CWRs in fixed zone is restricted, when the rail temperature changes compared to the stress-free temperature, the longitudinal strain along the rail will be zero, whereas the rail can expand and deform freely in the transverse and vertical directions. Thus, the transverse and vertical rail strains comprise two parts, namely the thermal strain and stress strain. In the following analysis, suppose that the temperature increase is positive and temperature decrease is negative, and the rail stress is positive under tension and negative under pressure (Fig. 1).

Suppose that a CWR is locked, the change of rail temperature relative to the fastening-down temperature is ΔT, and the longitudinal rail temperature strain (ε_{xT}) is zero. The longitudinal rail temperature stress (σ_{xT}) can then be expressed as

$$\sigma_{xT} = -\alpha \Delta T E, \tag{1}$$

where α refers to the rail's coefficient of linear expansion, which is generally 1.18×10^{-5}; E refers to the rail's elastic modulus, which is generally 2.06×10^{11} Pa [24–27].

As both the transverse and vertical rail temperature stresses (σ_{yT} and σ_{zT}) are zero, according to the mechanics of materials, the transverse and vertical rail thermal strains (ε_{yT} and ε_{zT}) can be expressed as

$$\varepsilon_{yT} = \varepsilon_{zT} = \alpha \Delta T - \left(\frac{\sigma_{xT}}{E}\right) v = (1 + v)\alpha \Delta T, \tag{2}$$

where v refers to Poisson's ratio of the rail, which is generally 0.3.

Theoretically, when the change in rail temperature is ΔT, the steel material constant E and v will change with ΔT, but these changes are negligible. Thus, E and v are taken as constant value. According to Eqs. (1) and (2), with the measured transverse or vertical rail strain, the longitudinal rail temperature stress (σ_{xT}) can be calculated according to Eq. (2), which can be expressed as

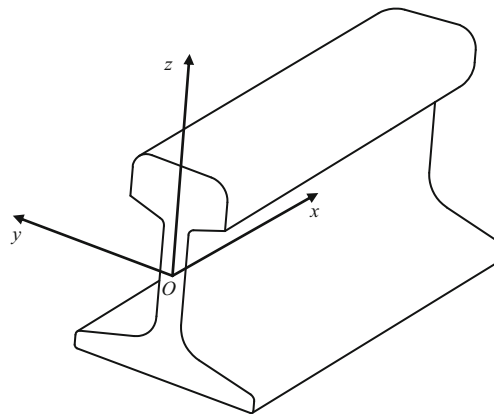$$\sigma_{xT} = -\frac{\varepsilon_{yT}}{1 + v} E = -\frac{\varepsilon_{zT}}{1 + v} E. \tag{3}$$

Fig. 1 Coordinate system of a locked long rail

⚛ Springer

J. Mod. Transport. (2018) 26(3):179–188

2.1.2 Stress–strain relations under additional longitudinal force

In fact, after a CWR is locked, the longitudinal rail stress is caused by rail temperature change. Moreover, rail creep, non-uniform distribution of rail resistance, and bridge expansion/contraction lead to an additional longitudinal force in the rail through the Poisson effect, and the corresponding transverse, vertical stresses and strains are generated. Taking a CWR on the simple supported beam bridge for example, the additional longitudinal force distribution along the rail is shown in Fig. 2.

Tensile or compressive deformation tends to occur under an additional longitudinal force. Therefore, the longitudinal strain (ε_{xF}) can be expressed as

$$\varepsilon_{xF} = \frac{F_f}{EA}, \tag{4}$$

where A refers to a cross-sectional area of the rail and F_f an additional longitudinal force in the rail. Here, it means contractility generated by beam temperature rise. Similarly, the additional force produced when the train is under the action of live road or braking can be called "flexure force" or "braking force."

The additional longitudinal stress in the rail (σ_{xF}) can then be expressed as

$$\sigma_{xF} = \frac{F_f}{A} = \varepsilon_{xF}E. \tag{5}$$

According to Eq. (5), after the longitudinal strain in the rail (ε_{xF}) is measured, the additional longitudinal stress in the rail (σ_{xF}) can be calculated.

Although the transverse and vertical additional stresses in the rail (σ_{yF} and σ_{zF}) are still zero under the additional longitudinal force, the transverse and vertical additional strains in the rail (ε_{yF} and ε_{zF}) is generated due to the effect of Poisson's ratio, which can be expressed as

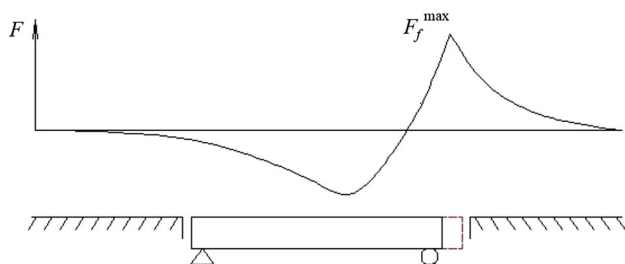$$\varepsilon_{yF} = \varepsilon_{zF} = -\nu\varepsilon_{xF}. \tag{6}$$

2.2 Bi-directional method improvement for rail stress measurement

In Sect. 2.1, the rail strain and stress under the rail temperature change and the action of additional force are analyzed, respectively. In fact, the longitudinal stress in CWRs which comes from both the change of rail temperature and various additional longitudinal forces, always changes alternately and dynamically, especially for the CWRs on bridges.

Suppose that the longitudinal stress in rail is σ_x, longitudinal strain is ε_x, and vertical strain in the rail is ε_z; then,

$$\sigma_x = \sigma_{xT} + \sigma_{xF}. \tag{7}$$

Substituting formulas (3) and (5) into Eq. (7), one has

$$\sigma_x = -\frac{\varepsilon_{xT}}{1 + \nu} + \varepsilon_{xF}E = \frac{\varepsilon_{xF} - \varepsilon_{zT}}{1 + \nu}E, \tag{8}$$

$$\varepsilon_x = \varepsilon_{xT} + \varepsilon_{xF} = \varepsilon_{xF}, \tag{9}$$

$$\varepsilon_z = \varepsilon_{zT} + \varepsilon_{zF}. \tag{10}$$

In addition, the total longitudinal stress (σ_x) can be expressed as

$$\sigma_x = \frac{\varepsilon_x - \varepsilon_z}{1 + \nu}E. \tag{11}$$

According to Eq. (11), the total longitudinal stress in the rail (σ_x) can be calculated when both the longitudinal strain in the rail (ε_x) and vertical strain (ε_z) are measured.

3 Rail stress monitoring device

3.1 Stress sensor module

According to the bi-directional strain method, we developed a rail stress monitoring device to realize the long-term and multi-point measurement of rail temperature stress [28], which includes a sensor module, a signal processing and transmitting module, etc. The sensor module comprises an H-shaped steel plate and a full-bridge strain gauge set on it. The material of steel plate is the same as that of the rail, with both ends fixed to the rail web (Fig. 3).
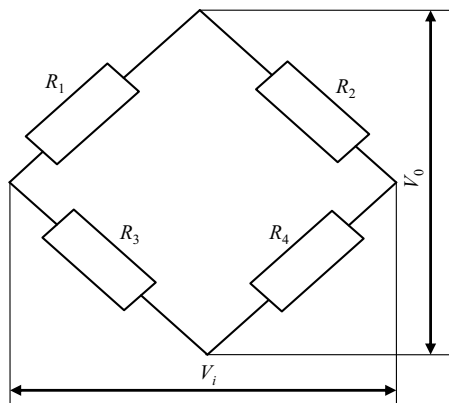

Fig. 2 Distribution of additional longitudinal force of rail in a bridge
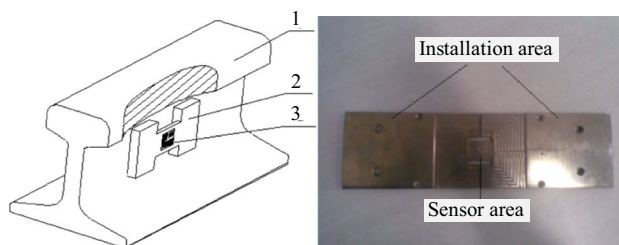
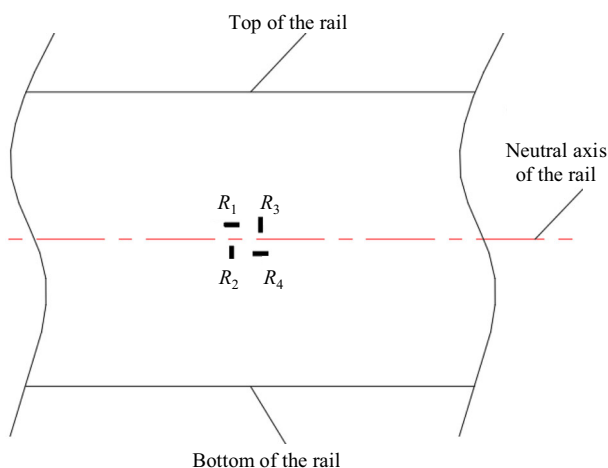1. Rail; 2 Steel plate; 3 Full-bridge strain gauge

Fig. 3 Rail stress monitoring device
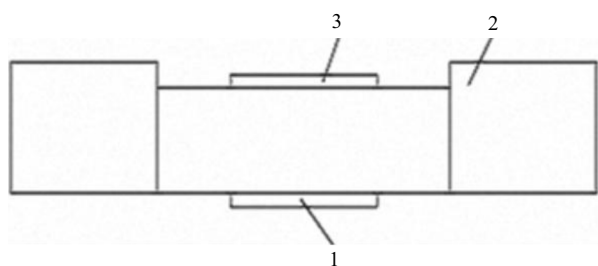
1. Rail; 2 Steel plate; 3 Full-bridge strain gauge

(a)

(b)

Fig. 4 Scheme for rail stress measurement: **a** bonding of full-bridge strain gauge, **b** schematic of electrical bridge

Slight deformation of the steel plate caused by the changes of temperature stress can decrease the accuracy of strain measurement. In view of this, the bottom of the sensor is designed as the "spindle" shape in order to effectively sense the rail strain; the two ends are large areas to fix and connect with the rail to ensure the relative fixation with the rail. The middle part is a thin and small sensing area. The design with a slightly thinner and narrower middle part reduces the strain loss of the steel plate caused by the elastic modulus of assembly glue being

lower than that of steel ingot, and ensures that the strain signals obtained by the full-bridge strain gauge are consistent with the rail strain. At the same time, the temperature sensor is attached to the steel plate to monitor the ambient temperature, which can show the internal temperature stress in rails. Figure 4 shows the bonding of a full-bridge strain gauge and the schematic of an electrical bridge.

3.2 Rail stress measurement process

As the resistance changes with the metal mechanical deformation, a full-bridge strain gauge with high sensitivity is used. When a piece of wire (length L, cross-sectional area S, resistance coefficient ρ, and resistance $R=\rho L/S$) becomes longer or shorter, the length (L), cross-sectional area (S) and resistance coefficient (ρ) will change accordingly. When the resistance variance is ΔR, the strain (ε) can be expressed as

$$\varepsilon = (\Delta R/R)/K, \tag{12}$$

where K refers to the sensitivity coefficient of the resistance strain gauge.

The full-bridge strain gauge A is fixed along the direction of the rail, as shown in Fig. 4(b). The two sets of strain meters of the full-bridge strain gauge should be perpendicular to each other and parallel to the direction of the rail. When the temperature stress of the rail changes, there is $R_1/R_2 = R_3/R_4$ because of isotropy. However, the rail and sleepers will restrict the prolongation in the direction of the rail; then, a certain stress (σ) of the rail will be generated which will cause a certain strain $\varepsilon=\sigma/E$ in the direction of the rail.

When the input voltage of the full-bridge strain gauge is V_0, the bridge voltage (V_i) can be expressed as

$$V_i = [R_1/(R_1 + R_2) - R_3/(R_3 + R_4)]V_0. \tag{13}$$

For the strain gauge A, when the test piece (cross-sectional area S) is measured under a load F, the change in the resistance R (ΔR) can be obtained by measuring the change in the bridge voltage V_i (ΔV_i), and the strain (ε) can also be measured. Its stress (σ), according to the stress–strain relationship, can be expressed as

$$\varepsilon = \Delta V_i R_2(R_3 + R_4)/(V_0 R_4),$$
$$\sigma = E\varepsilon. \tag{14}$$

The sensor module outputs a voltage signal after measuring the minor deformation of the rail caused by the change of stress. Then, the signal processing and transmission module amplifies and modulates this signal after receiving it. The signal data will be stored and then transmitted to the receiving device regularly through wireless transmission by a transmitter module in order to
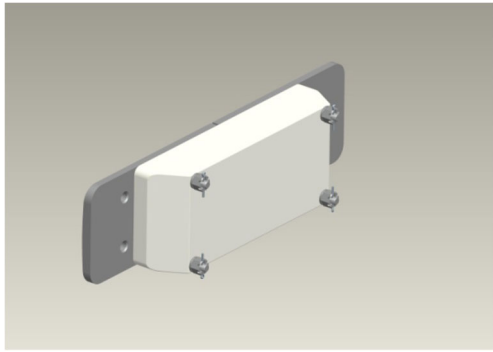
🌊 Springer

J. Mod. Transport. (2018) 26(3):179–188

realize long-term and multi-point monitoring of changes in rail stress.

The sensor module and the signal processing/transmitting module are packaged in a box for the sake of easy installation and protecting the device from damage (as shown in Fig. 5).

4 Correction of measured results

4.1 Analysis of measured results correction due to changes in rail temperature

Supposing that the temperature change for a rail is ΔT, the elongation (ΔL_T) of the sensor can be expressed as (Fig. 6):

$$\Delta L_T = \alpha(L_1 + L_2)\Delta T, \quad k_1 = \frac{EA_1}{L_1}, \quad k_2 = \frac{EA_2}{L_2}. \quad (15)$$

Suppose that the force acted on sensor is F_{ST}.
Then, in the free state

$$\Delta L_{1T} = \frac{F_{ST}L_1}{EA_1}, \quad \Delta L_{2T} = \frac{F_{ST}L_2}{EA_2}, \quad \Delta L_{1T} + \Delta L_{2T} = \Delta L_T. \quad (16)$$

And under fixed constraints,

$$F_{ST} = \frac{\alpha(L_1 + L_2)\Delta TEA_1 A_2}{L_1 A_2 + L_2 A_1}. \quad (17)$$

Supposing that the total longitudinal stress, total longitudinal strain, and total vertical rail strain within the bonding range of the sensor strain gauge are σ_{xST2}, ε_{xST2} and ε_{zST2}, respectively, then

$$\sigma_{xST2} = \frac{F_{ST}}{A_2} = \frac{\alpha(L_1 + L_2)\Delta TEA_1}{L_1 A_2 + L_2 A_1},$$

$$\varepsilon_{xST2} = \alpha\Delta T - \frac{\alpha\Delta T(L_1 + L_2)A_1}{L_1 A_2 + L_2 A_1}, \quad (18)$$

$$\varepsilon_{zST2} = \alpha\Delta T + \frac{\alpha\Delta T(L_1 + L_2)A_1}{L_1 A_2 + L_2 A_1}v.$$

The strain (ε_{ST}) under the change in rail temperature can then be expressed as

$$\varepsilon_{ST} = 2(\varepsilon_{xST2} - \varepsilon_{zST2}) = -2(1 + v)\frac{\alpha\Delta T(L_1 + L_2)A_1}{L_1 A_2 + L_2 A_1}. \quad (19)$$

As concluded from above, for a long rail in a fixed continuously welded area, when the sensor section is uniform (i.e., $A_1 = A_2$), the longitudinal strain (ε_{xST2}) within the bonding range of the strain gauge will be zero. Therefore, for such rail-stress-monitoring sensors, the measured strain (ε_{ST}) should be divided by a correction coefficient (κ_1). The correction coefficient is calculated according to the following equation:

$$\kappa_1 = \frac{(L_1 + L_2)A_1}{L_1 A_2 + L_2 A_1}. \quad (20)$$

4.2 Analysis of measured corrected results with sensor under additional longitudinal force

When an additional longitudinal force (F_f) is applied to the rail, the analysis method presented in Sect. 4.1 is adopted. Considering the non-uniformity of the sensor section, the measured strain (ε_{SF}) under the additional longitudinal force should also be divided by an additional force correction coefficient (κ_2).

4.3 Analysis of corrected measurement results in total rail stress

In fact, when the temperature range is ΔT, and an additional longitudinal force (E_f) is applied to the rail, the measured total strain (ε_S) can be expressed as

$$\varepsilon_S = \varepsilon_{ST} + \varepsilon_{SF} = \frac{2(1 + v)(L_1 + L_2)A_1}{L_1 A_2 + L_2 A_1}\left(\frac{F_f}{EA} - \alpha\Delta T\right), \quad (21)$$

where

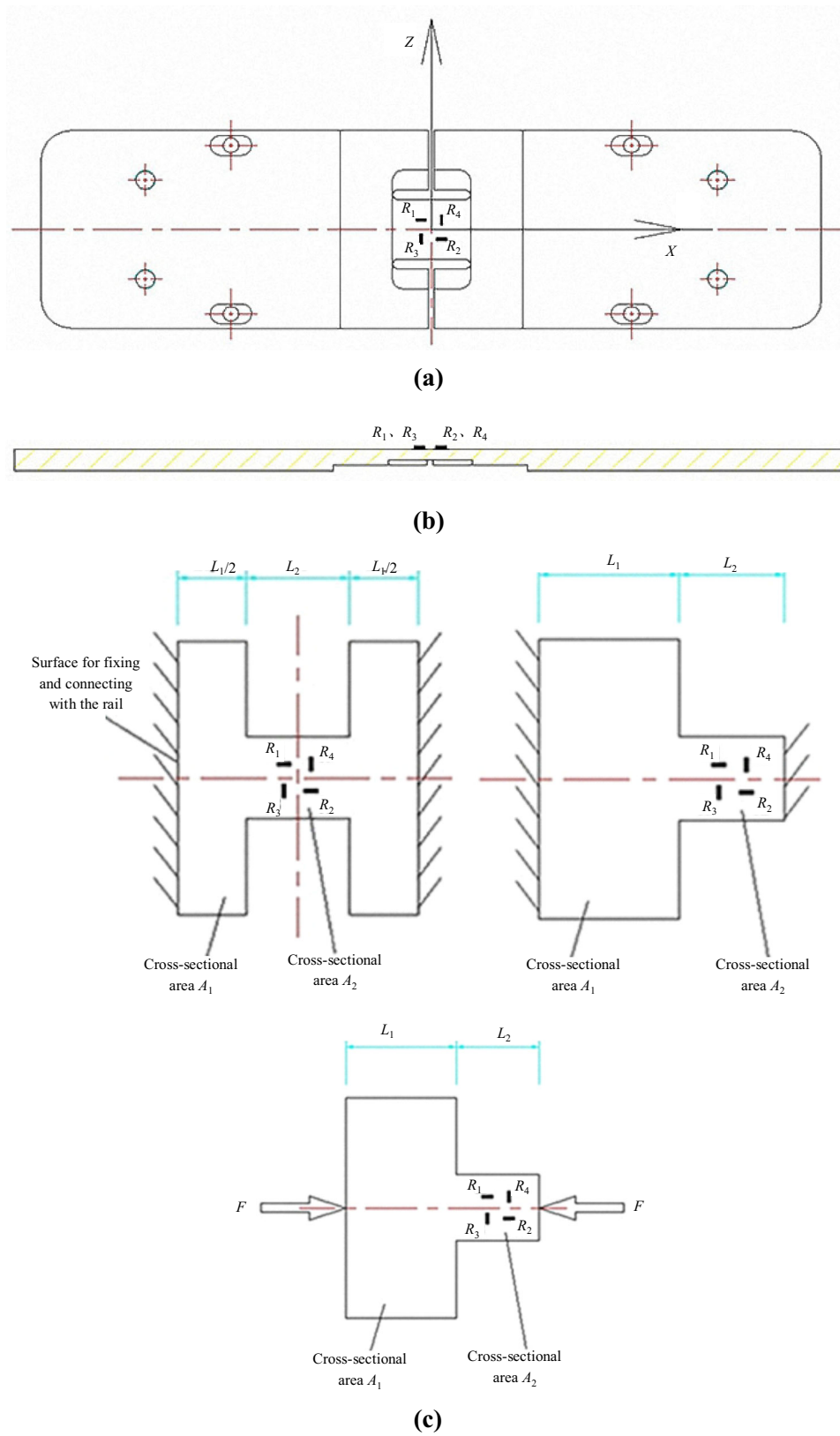$$F_f = \left[\frac{\varepsilon_s}{2(1 + v)k} + \alpha\Delta T\right]EA. \quad (22)$$

(a)

(b)

(c)

Fig. 6 Schematic diagram of the test device on a steel plate. Front (**a**) and top (**b**) views of steel plate, and (**c**) designed size of the sensor module

🕮 Springer

J. Mod. Transport. (2018) 26(3):179–188

5 Test of rail stress using monitoring sensor

5.1 Test of basic temperature stress in rail

A temperature was set and an axial force was loaded on a rail installed with a stress-monitoring sensor (Fig. 7). The measured results were compared with the theoretical solutions.

The CHN60 rail with a length of 60 cm was used in the test, which is based on the distance of 60 cm between consecutive rail fasteners in Chinese Code for Design of Railway Continuous Welded Rail TB 10015-2012(J 1586-2013). To simulate the locked state of CWR, we set the universal testing machine (1,000 kN) in a fixed state and installed the rail between the two loading heads of the machine to avoid longitudinal strain during the test. In addition, we used external heat source to heat the rail, and measured the rail stress at different temperatures. The test device is shown in Fig. 8.

Fig. 7 Rail stress-monitoring sensor

Fig. 8 The universal testing machine in a temperature box

5.2 Test of additional longitudinal stress in rail

An axial load was exerted on the test rail by a jack. Then, the additional longitudinal stress was measured with the rail stress monitoring sensor installed on the rail web [29]. The measured additional stress was compared with the theoretically calculated additional stress.

5.3 Test results

5.3.1 Test of basic temperature stress in rail

The initial rail temperature was set as $T_0 = 0$ and T_{ci} the actual rail temperature. For the CWRs, it is usually assumed that the stress-free temperature is a constant value in the existing CWR design and calculation. The author thus conducts relevant research based on this assumption. When the rail temperature rises from T_0 to T_{ci}, the rail stress (σ_i) is

$$\sigma_i = \alpha E(T_{ci} - T_0), \tag{23}$$

where α refers to the rail's coefficient of linear expansion and E the rail's elastic modulus.

Using the rail-stress-monitoring sensor, the longitudinal force in the rail was measured under different temperatures and the results were compared with theoretical values (Table 1).

A comparison was made between the rail stress measured with the stress sensor under different changes in the temperature and theoretical values (Fig. 9).

As can be seen from Fig. 9, the three lines basically overlap, showing the following facts.

1. There are minor errors between the measured rail stresses under different changes in temperature, and the maximum error rate is 8.76%.
2. Two groups of the test results are in good agreement, demonstrating that the rail stress monitoring sensor works in a stable and reliable state.

As Fig. 10 shows, the measuring errors increase gradually with the change in temperature. For example, when the change in rail temperature reaches 10 °C, the error result is approximately 1.5 MPa. When the rail temperature stresses are measured with resistance strain gauges, the thermal strain of the strain gauges should not be neglected. As previously mentioned, with sensitive directions being perpendicular to each other, the resistance wires of full-bridge gauges were parallel and perpendicular to the directions of the rail, thus the thermal strains of the four strain gauges were able to counteract with each other. However, considering the uneven distribution of the actual temperature for the rail section, measuring errors still

Table 1 Comparison between the measured temperature stresses in rail and theoretical ones

No.	Initial rail temperature T_0 (°C)	Actual rail temperature T_{ci} (°C)	Stress measured (MPa)	Theoretical stress (MPa)	Error (%)
1	25	27	4.7	4.9	4.08
2	25	29	10.3	9.7	6.19
3	25	31	16.0	15.6	2.56
4	25	33	21.1	19.4	8.76
5	25	35	26.3	24.3	8.23
6	26	28	4.8	4.9	2.04
7	26	30	10.5	9.7	8.25
8	26	32	14.4	15.6	7.69
9	26	34	20.3	19.4	4.64
10	26	36	25.7	24.3	5.76
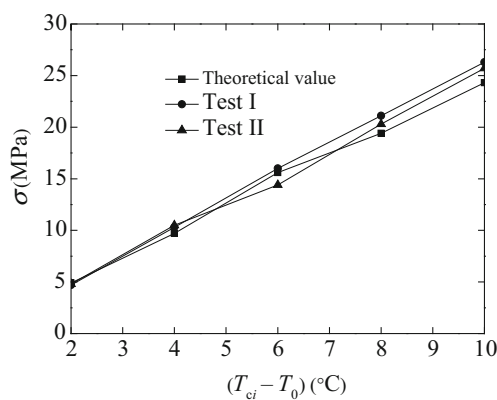
Fig. 9 Measured temperature stresses in rail
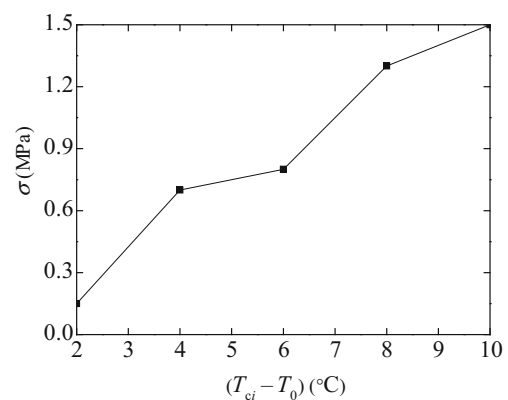
Fig. 10 Analysis of measuring error of rail temperature stress

existed when measuring the basic temperature stresses in the rail.

5.3.2 Test for additional longitudinal rail stress

A certain axial force was exerted on the rail installed with the sensor. Next, pressure (F_i) was added gradually on both ends of the rail by a certain grading. Then, the additional longitudinal stresses measured in the rail were recorded. Note that the rail temperature should not be changed when only measuring the additional longitudinal stresses of the rail. Afterward, a set of additional longitudinal stresses, which were measured in the rail, was selected (Table 2).

A comparison was made between the additional longitudinal stresses of the rail measured and the theoretical values (Fig. 11). The test condition is the same as above.

According to the results for the additional longitudinal stresses measured in the rail (Fig. 11), the results from the stress-measuring sensor under different axial forces basically match the theoretical values. The measuring errors under different axial loads are also shown in Fig. 12.

According to Fig. 11, a higher axial load of the rail accompanies with a higher measuring error. When the load is 210 kN, the error is approximately 1.9 MPa, nearly 7% of the additional longitudinal stress of the rail. As for the bi-directional strain method mentioned in this paper for measuring rail stresses, although the temperature values of the four full-bridge strain gauges can offset each other and the measuring errors caused by the flexural strain can be eliminated at the same time, there still may be some unbalanced flexural strain causing errors in the measured results, because the field conditions can not be fully simulated in the laboratory test.

5.4 Analysis of measured results

The above test results show that the measurement of longitudinal rail stresses performed based on the bi-directional strain method is basically feasible. The rail temperature stress and additional longitudinal force measured with the rail stress monitoring sensor are close to the theoretical values. In the measurement of longitudinal rail stress,

🍂 Springer

J. Mod. Transport. (2018) 26(3):179–188

Table 2 Results for additional longitudinal stresses in rail

Exerted axial force F_i (kN)	Stress measured (MPa)	Theoretical stress F_i/A (MPa)
0	0	0.0
10	0.9	1.3
30	2.9	3.9
50	5.4	6.5
70	7.7	9.0
90	9.9	11.6
110	12.1	14.2
130	14.9	16.8
150	17.1	19.4
170	19.2	22.0
190	21.9	24.5
210	24.6	27.1
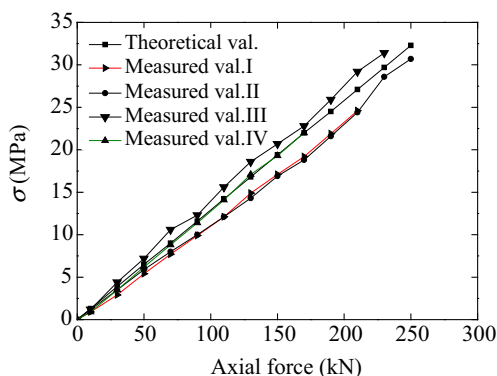
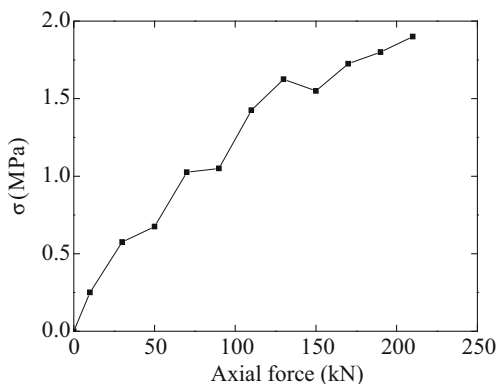**Fig. 11** Additional longitudinal stresses measured in rail

Fig. 12 Analysis of measuring errors of additional longitudinal stresses in rail

measuring points are chosen on-site for real-time monitoring, and it is necessary to install the rail at the zero-temperature stress state to eliminate the existing rail stress in the early operation stage.

6 Conclusions

By analyzing the stress–strain relations CWRs, this paper presented a measuring method for longitudinal rail stress based on the bi-directional strain method, developed a monitoring device of rail stress for long-term and multi-point measurements, and provided relevant experimental verification and analysis. Furthermore, the following conclusions have been reached:

1. For rail stress–strain states under different restriction conditions, according to the bi-directional strain method for measuring the stress of CWRs, the total longitudinal rail stress can be calculated with the measured total longitudinal strain and total vertical strain.

2. When the stress sensor module is used for measuring the longitudinal force in CWRs, in light of measurement errors caused by sensor sections, we put forward a correction equation that can improve the accuracy of the measured results under different stress conditions.

3. According to the test, the measured rail temperature force and additional longitudinal force are similar to the theoretical values. When the change in rail temperature is 10 °C, the measuring error of the rail temperature stress is approximately 1.5 MPa. When the axial load is 210 kN, the measuring error of the additional axial stress will be approximately 1.9 MPa, nearly 7% of the additional longitudinal stress of the rail.

References

1. Cai C-B (2003) Calculation of additional longitudinal forces in continuously welded rails on super-large bridges of high-speed railways. J Southwest Jiaotong Univ 38(5):609–614 **(in Chinese)**
2. Xu Q-Y, Chen X-F, Li S-D (2006) Study on the additional longitudinal forces transmitted between continuously welded rails and high-speed railway bridges. China Railway Sci 27(3):8–12 **(in Chinese)**
3. Lu Y-R (2004) Research and application of CWR. China Railway Publishing House, Beijing, pp 140–188 **(in Chinese)**

4. Rail Safety & Standards Board (2008) Management of stressed continuously welded track-rail stress-free temperature measurement techniques. RSSB Research and Development Programme, London

5. Harrison H, McWilliams R, Kish A (2007) Handling CWR thermal forces. Railway Track and Structures, New York, pp 42–45

6. Bartosiewicz A et al (1999) Experiences in the application of ultrasonic stress measurements for railway industry. Foreign Rolling Stock 6:31–36

7. Wang P, Gao Y-L, Yang YR et al (2013) Experimental studies and new feature extractions of MBN for stress measurement on rail tracks. IEEE Trans Magn 8(49):4858–4864 **(in Chinese)**

8. Gokhale S (2007) Determination of applied stresses in rails using the acoustoelastic effect of ultrasonic waves. Texas A&M University, Texas

9. ASME (2007) A novel method for estimating the neutral temperature of continuously welded rails. In: ASME rail transportation division fall technical conference, Sep 11–12, 2007, pp 105–115

10. Peng X-D, Ding J-X (2006) Study on monitoring thermal stresses in continuously welded rails with LCR waves. J Univ Electron Sci Technol China 10(35):844–847 **(in Chinese)**

11. Filograno ML, Corredera GP et al (2012) Real-time monitoring of railway traffic using fiber bragg grating sensors. IEEE Sens J 12(1):85–92

12. Tunna J (2000) Vertical rail stiffness equipment (VERSE) trials. Letter Report for Vortex International Transportation Technology Center, Inc. (TTCI), Pueblo, CO

13. Kelleher J, Prime MB, Buttle D et al (2003) The measurement of residual stress in railway rails by diffraction and other methods. J Neurosci Res 11(4):187–193

14. Hayes AP (2008) MAPS-SFT, a new tool in the infrastructure manager's toolbox. In: 2008 4th IET international conference on railway condition monitoring, 18–20 June 2008, ISSN: 0537-9989

15. Hurlebaus S (2011) Determination of longitudinal stress in rails. Final Report Safety IDEA Project 15, Transportation research Board, Washington, DC

16. Nucera C, Lanza di Scalea F (2014) Nondestructive measurement of neutral temperature in continuous welded rails by nonlinear ultrasonic guided waves. J Acoust Soc Am 136(5):2561–2574

17. Zhu X, Lanza di Scalea F (2017) Thermal stress measurement in continuous welded rails using the hole-drilling method. Exp Mech 57:165. https://doi.org/10.1007/s11340-016-0204-8

18. Song X-W (2012) Error analysis and improvement of rail longitudinal force measurement by electrical measuring method for strain. Dalian University of Technology, Dalian **(in Chinese)**

19. Zhang F-S (2012) Error analysis and improvement in monitoring the stress-free temperature of continuous welded rails by strain-temperature measurement method. Dalian University of Technology, Dalian **(in Chinese)**

20. Feng S-M (2012) Monitoring and analysis of longitudinal forces from CWRs in ballastless tracks on long spanning bridges for high-speed railways. East China Jiaotong University, Nanchang **(in Chinese)**

21. Feng S-M, Lei X-Y, Zhang P-F et al (2011) Remote monitoring and analysis of additional contractility from CWRs on bridges. J East China Jiaotong Univ 28(2):1–5 **(in Chinese)**

22. AEA Technology Rail (2006) Findings from the investigation of SFE measurement techniques. AEA Technology Rail, London

23. Li Y-H (2013) Research on wireless monitoring system hardware for distributed rail stress. Dalian University of Technology, Dalian **(in Chinese)**

24. Wang P, Xie K, Shao L et al (2015) Longitudinal force measurement in continuous welded rail with bi-directional FBG strain sensors. Smart Mater Struct 25(1):1–10

25. Wang P, Xie K, Chen R, Shao L et al (2016) Test verification and application of a longitudinal thermal force testing method for long seamless rails using FBG strain sensor. J Sens. Article ID 3917604

26. Wang P, Xu J, Xie K et al (2016) Numerical simulation of rail profiles evolution in the switch panel of a railway turnout [J]. Wear 366–367:105–115

27. Wang B, Xie K, Xiao J, Wang P (2016) Test principle and test scheme of longitudinal force in continuous welded rail using resistance strain gauge. J Southwest Jiaotong Univ 51(1):43–49

28. Ding J-X (2012) Monitoring device for rail thermal stress, China, CN201120140230. X[P]. 2012-01-11 **(in Chinese)**

29. Yan B, Dai G, Guo W, Xu Q (2015) Longitudinal force in continuously welded rail on long-span tied arch continuous bridge carrying multiple tracks. J Central South Univ 22(05):2001–2006

🍩 Springer

J. Mod. Transport. (2018) 26(3):179–188